Presented at 1994 International Mechanical Engineering Congress and Exposition. Fire, Combustion, and Hazardous Waste Processing, Nov. 6-11, 1994, Chicago, IL. Sponsored by the Heat Transfer Division, ASME.

HTD-Vol. 296, Fire, Combustion and Hazardous Waste Processing
ASME 1994

SIMULATING THE EFFECT OF FLAT BEAMED CEILING ON DETECTOR AND SPRINKLER RESPONSE

Glenn P. Forney, Richard W. Bukowski, and William D. Davis
Building and Fire Research Laboratory
National Institute of Standards and Technology
Gaithersburg, Maryland

ABSTRACT

This paper documents a portion of the work performed during the first year of the International Fire Detection Research Project sponsored by the National Fire Protection Research Foundation (NFPRF). The first task was to confirm that fire sensor response can be evaluated using computational data obtained from numerical simulations. A field model was verified for this application by showing that its temperature predictions match experimental results obtained earlier by Heskestad and Delichatsios. This paper concentrates on the second task which was to perform a parameter study to show the effect of sensor response under beamed ceilings for various geometries and fire sizes. One question that is addressed is under what conditions can sensors be located on beams rather than in beam pockets. Time to sensor activation contour plots are presented that address this question. Twenty cases were run for various fire sizes, beam depths, beam spacings and ceiling heights. These data are summarized and recommendations are made on placing sensors in rooms with beamed ceilings.

INTRODUCTION

The rapid activation of fire detection and suppression systems in response to a growing fire is one of the important factors required to provide for life safety and property protection. Rapid activation requires that the sensors be located at an optimal distance both beneath the ceiling and radially from the fire. Ceiling obstructions to the movement of heat and smoke such as beams and joists must be taken into account when the system is designed, but little quantitative information is contained in the standards.

Experiments were performed by Heskestad and Delichatsios in the late seventies in order to evaluate the response of fire sensors under flat ceilings (see Heskestad and Delichatsios [1, 2]) and beamed ceilings (see Heskestad and Delichatsios [3, 4]). Quoting from Heskestad and Delichatsios [3],

> "The major objective of this work was to generate graphical and tabular presentations of the environmental data in both physical forms and "reduced" forms, the latter allowing extrapolation of the data to arbitrary combination of ceiling heights and fire-growth rates. A second objective was to confirm previously established methods of predicting the response of fire sensors from the environmental data and subsequently to determine optimum spacing of fire sensors under large beamed ceilings."

These goals can also be realized by using numerical simulations to produce the data from which graphical and tabular presentations are derived. It was shown in Forney et al. [5, 6] that numerical simulations could predict experimental temperature measurements given in Heskestad and Delichatsios [4]. This paper describes a series of numerical simulations performed to study the effect of fire size, beam depths, beam spacing and ceiling heights on smoke flow under beamed ceilings. These results were analyzed in order to determine how sensor placement can be influenced by the above room/fire configurations. Ultimately, the goal of this work is to provide a basis for sound recommendations for modifications to the Standard on Automatic Sprinklers (NFPA 13) and the National Fire Alarm Code (NFPA 72).

MODELING ASSUMPTIONS

Conservation Equations

The modeling technique used to simulate smoke flow is to divide the region of interest into a collection of small rectangular boxes or control volumes. The conditions in each control volume are initially ambient. Heat is then released in several control volumes over time. The resulting flow or exchange of mass, momentum and energy between control volumes is determined so that these three quantities are conserved. The momentum conservation equations are equivalent to Newton's second law of motion and are sometimes referred to as the *Navier-Stokes* equations. The energy conservation equation is equivalent to the first law of thermodynamics. These fluid flow equations are expressed mathematically as a set of simultaneous, non-linear partial differential equations. After being discretized, the resulting finite volume[1] equations are solved iteratively using a variant of Newton's method for computing coupled non-linear algebraic equations.

Turbulence

We used the standard $k - \epsilon$ model of Launder and Spalding [7] to model turbulence. We ran several cases comparing various forms of the $k - \epsilon$ turbulence model and did not find any significant difference in the temperature predictions.

Compressibility

It was assumed that the fluid was air and that it was compressible. This assumption may be relaxed in the future, subject to verification, by 1) neglecting the propagation of pressure waves (assuming that the speed of sound is infinite) or 2) assuming that density variations are only important in the momentum equation (Bousinesq approximation). Making either of these assumptions will improve the speed of the model and hence shorten either run times or allow for a more refined grid.

Heat Transfer

All solid surfaces were assumed to be adiabatic. Clearly heat is transferred from the gas to the walls. This assumption will result in warmer gas temperature predictions than without it since no convective heat transfer occurs between the gas and the walls. For wall materials that are nearly insulating, the wall temperatures will quickly rise to the gas temperature which reduces the heat transfer. The time period over which a parcel of gas is in contact with a wall surface is on the order of seconds[2]. From these two observations we conclude that the adiabatic assumption is reasonable.

Radiation effects were not included in the calculation except that only a fraction of the heat release rate was assumed to contribute to convective heating of the smoke and air. The rest of the heat was considered to be radiated away. This assumption produces the greatest error since 1) the fraction of heat radiated away is unknown and 2) the gas temperatures are very sensitive to fire size. The radiative loss fraction, χ_r, is then a calibration parameter similar to the ones used for the turbulence models discussed above.

Boundary Specifications

Six boundary conditions are required, one for each of the six bounding surfaces that define the region begin modeled. The floor and beamed ceiling are assumed to be solid. A no-slip boundary condition was assumed. The two surfaces opposite the fire are constant pressure boundaries. The two surfaces nearest the fire are specified as symmetric boundaries. The two symmetry planes split the experimental region into four regions.

Fire

The NFPA 72E standard [8] defines *fire size*[3] in terms of how long it takes a 't^2' or quadratic fire to reach 1.055 MW (1000 Btu/s). If

$$\dot{Q}(t) = 1.055(t/t_{\text{size}})^2$$

is the energy release rate of a fire at time t then the NFPA 72E standard [8] defines t_{size} for a slow fire to satisfy $t_{\text{size}} > 400$, for a medium fire, $150 < t_{\text{size}} < 400$ and a for a fast fire to be $t_{\text{size}} < 150$. The fires modeled in this paper were then assumed to have a heat release rate of the form

$$\dot{Q}(t) = 1.055(1 - \chi_r)(t/t_{\text{size}})^2/4$$

where χ_r is the fraction of heat going to radiation, t_{size} takes on values of 150 seconds for fast fires, 275 seconds for medium fires and 400 seconds for slow fires. In Forney et al. [9], it was found that $\chi_r = 0.35$ gave the best agreement between the numerical predictions and experiment. The number 4 arises by symmetry since only one of four quadrants are simulated and it is assumed that the fire contributes equally to each quadrant.

MODEL VERIFICATION

Numerical field modeling can effectively complement laboratory experiments as long as the two approaches give consistent results in a comparable time. This section present results that show that the two approaches are in good agreement. A typical 5 minute simulation using 3105 control volumes took approximately 48 hours of computer time on a Silicon Graphics 4D35 work station. Grids for the parameter study were refined in order to better resolve the ceiling jet near the beams. These simulations, using 6555 control volumes, took approximately 36 hours on an Silicon Graphics R4000 Indigo. This Indigo is approximately 2.5 times

[1] The unknowns in finite volume equations are at the center of the control volume while the unknowns in finite difference equations are at the edge or corners.

[2] scale length of ceiling / fluid velocity = transit time $\approx$ 10 m / 2 m/s = 5 s

[3] While NFPA 72E refers to this as fire size it is more correctly referred to as a fire growth rate.

faster than the 4D35. For simple grids, it usually takes a few hours to set up a case. Several runs are required to insure that a case is set up correctly. Thus the cumulative time for setting up and running a field model is shorter than the time required to set up and perform a comparable laboratory experiment. Therefore field modeling is a good approach for solving these types of problems.

Six beam configurations were investigated experimentally by Heskestad and Delichatsios in [3, 4]. Three configurations consisted of beams with dimensions 0.305 m (1 ft) by 0.152 m (6 in) with 0.61, 1.22 and 1.83 m (2, 4 and 6 ft) on center (OC) spacing. The other three configurations consisted of beams with dimensions 0.61 m (2 ft) by 0.305 m (1 ft) with 1.22, 2.44 and 3.66 m (4, 8 and 12 ft) OC spacing. Each of these six configurations consisted of a suspended beamed ceiling with no walls and a solid floor. The ceiling was moved to keep the distance between the top of the crib and the bottom of the beams at 2.44 m (8 ft). Therefore, the 0.305 (1 ft) beam depth experiments had a ceiling height of 3.05 m (10 ft) while the 0.61 (2 ft) beam depth experiments had a ceiling height of (11 ft). Three experiments were performed for each configuration. An additional three experiments were performed with draft curtains in addition to the beams.

Comparisons for a short beam spaced experiment, experiment 4, are presented here. A medium beam spaced experiment, experiment 16, were also compared and gave similar results. The large beam spaced experiments, 19, 20 and 21, required more grids to simulate two channels than the short and medium case. Experiment 4 consisted of ceiling beams spaced 1.22 m (4 ft) apart with a depth of 0.305 m (1 ft). Experiment 16 consisted of ceiling beams spaced 2.44 m (8 ft) apart with a depth of 0.61 m (2 ft).

1.22 m (4 ft) OC Spaced Experiment

Figure 1 shows a schematic of the top view for the setup for experiment 4. This figure corresponds to Figure 1b in Heskestad and Delichatsios [4]. The numbers denote temperature sensor locations. These sensors are located 0.152 m (6 in) below the ceiling. The ceiling height is 3.05 m (10 ft). The fire source, a wood crib, was located at position 0 as a point source of energy.

The portion of the experiment simulated using the field model is outlined with the small interior rectangle in Figure 1. The simulated region includes four flow channels. A channel refers to the space near the ceiling between adjacent beams. The beams tend to isolate or channel the smoke flow. Therefore, the temperature tends to drop more rapidly (towards ambient) across channels than within a channel. Because of this, four channels are sufficient to simulate the main features of the experiment. The vertical grid dimensions near the floor are 0.61 m (2 ft) while grids near the ceiling have a vertical dimension of 0.305 m (1 ft). The horizontal grid dimensions are for the most part 0.305 × 0.305 m (1 ft × 1 ft). The grids are smaller near the beams to better resolve the flow and to simulate the correct beam spacing.

Figure 2 shows temperature comparisons for location 0 (above the fire), location 17 (in first channel), location 1 (under the beam

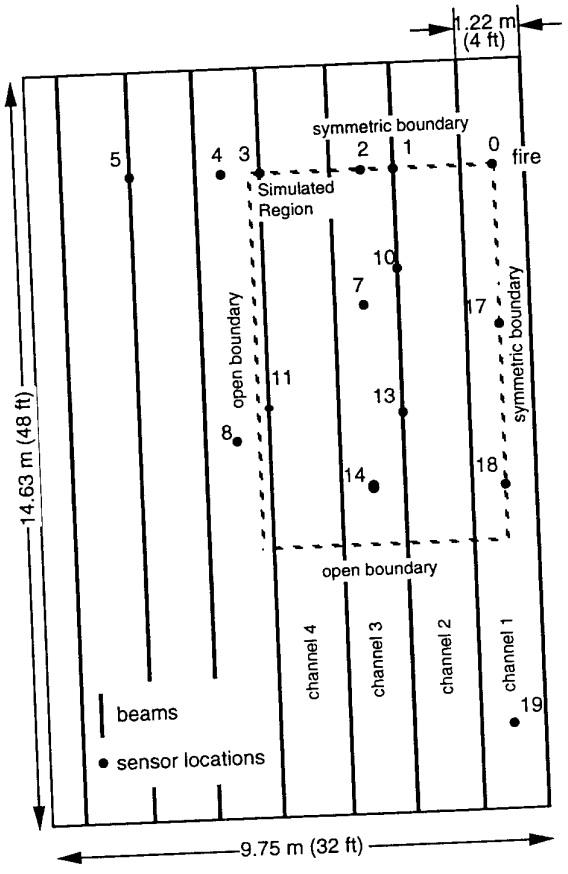

FIGURE 1: Physical Configuration for 4 ft On Center Spaced Beam

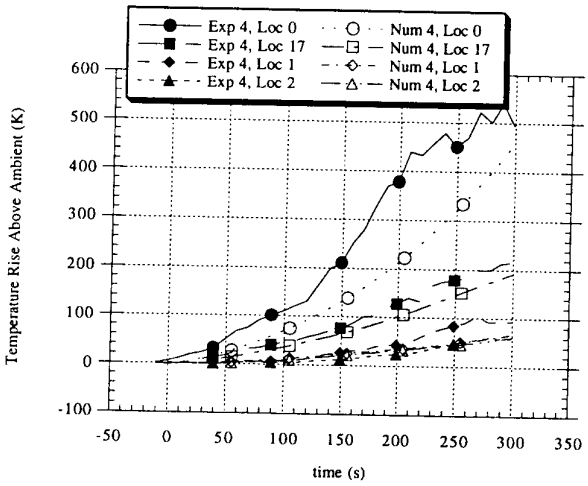

FIGURE 2: Comparison of Numerical and Experimental Temperatures at Sensor Locations 0 (over the fire), 17 (in first channel) , 1 (under the second beam) and 2 (in the third channel) for the 4 ft On Center Spaced Beam Experiment

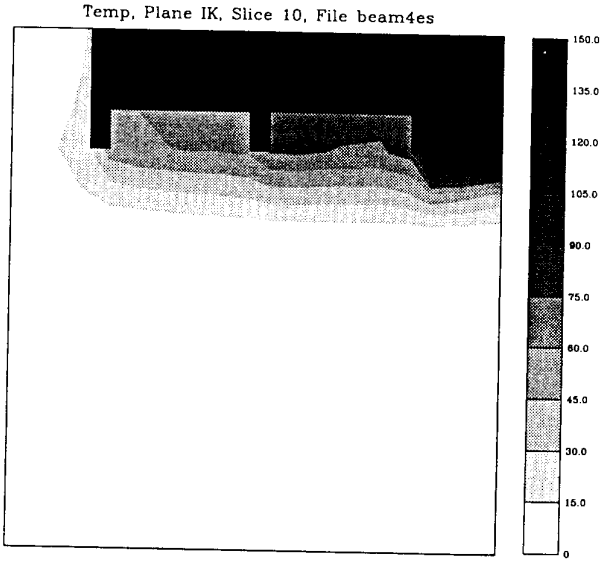

FIGURE 3: Shaded Temperature Rise Contours (° C) for the 4 ft On Center Spaced Beam Experiment in a Vertical Plane Perpendicular to the Beams 3.05 m (10 ft) from the Fire at 300 seconds

separating the second and third channel) and location 2 (in the third channel). Temperature comparisons for other locations (18, 10, 13, 7 and 14) are similar to those shown in Figure 2. Temperature comparisons were made for all locations within the shaded rectangle except for locations 3 and 11. These locations are under the beam in the fourth channel. The experimentally measured temperature rises were approximately 10 °C (18 °F) at 300 seconds.

The field model calculates the temperatures at the center of each grid cell. The temperature at the instrument locations were calculated by linearly interpolating this data using the B3INK/B3VAL software of Boisvert et al. [10] which implements tensor product B-spline interpolation algorithms of deBoor [11, 12].

The agreement between numerical and experimental temperature measurement directly over the fire is not good. This discrepancy is likely caused by radiation heat transfer not accounted for in the experimental temperature measurement. The flame height was estimated to be 2.8 m (9.2 ft) using Heskestad's flame height correlation[13], $L = -1.02 + 0.235\dot{Q}^{2/5}$ and assuming that $\dot{Q} = 1000kW$. This is consistent with Figure 10 on page 25 of Heskestad and Delichatsios [4] which shows a photograph of a 0.61 m (2 ft) beam depth experiment 6 minutes into a simulation. Noting that the flame tip reaches the bottom of the beams, it can be inferred that the flame height is 2.74 m (9 ft).

Temperature comparisons at other locations, are good. The field model successfully predicts quantitatively the temperature rise with time and the temperature drop off that occurs going from the first channel containing the fire to the third channel. The experimental data used for the comparison was obtained from Heskestad and Delichatsios [3].

Figures 3 and 4 show how the hot gasses generated by the fire plume are channeled by the beams. The fire in Figure 4 is located in the upper right corner. The shaded contours represent the temperature rise in °C above ambient. The contours in Figure 3 lie in a vertical plane perpendicular to the beams 3.05 m (10 ft) from the fire. The contours in Figure 4 lie in a plane parallel to the floor 0.152 m (6 in) below the ceiling. Similar contour plots with shorter beam depths show, as expected, smoke flow that is less channeled.

CASE STUDY

Scope

A series of numerical experiments were performed to study the effects of beam depths, beam spacing, ceiling heights and fire size on the distribution of heat and smoke near the ceiling and their effect on sensor activation. Five series of numerical simulations were performed. The first four series varied one parameter while leaving the other parameters fixed. The fifth series consisted of several cases modeling enclosed spaces. The base case, similar to experiments 4, 5 and 6 in Heskestad and Delichatsios [3], consisted of a 't^2' fire which reached 1.055 MW (1000. Btu/s) in 275 seconds, a ceiling height of 3.36 m (11 ft) and beam depths of 0.305 (1 ft).

Five cases were run with varying beam depths. The depths consisted of 0.0 m (0 in), 0.10 m (4 in), 0.20 m (8 in), 0.305 m (1 ft) and 0.61 m (24. in). Six cases were run varying ceiling height.

These temperatures and activation times were calculated every 5 seconds for each control volume throughout the 300 second simulations. Temperature contour plots are produced at any time by linearly interpolating temperature data at times in the dump file that bracket the desired time. Activation times for gas temperature devices are calculated by noting the *first* time the gas temperature reaches the temperature T_{crit}. For smoke detectors, T_{crit} is taken to be 13 $^{\circ}C$ above ambient. For heat detectors, T_{crit} is taken to be 57.2 $^{\circ}C$ (135 $^{\circ}$ F). The temperature of the sensing element such as found in heat detectors and sprinklers is estimated using the differential equation developed in Heskestad and Delichatsios [14]

$$\frac{dT_L}{dt} = \frac{\sqrt{S(t)}}{\text{RTI}} \left(T_g(t) - T_L(t)\right), \qquad (1)$$

$$T_L(0) = T_g(0)$$

where T_L, T_g are the link and gas temperatures in $^{\circ}C$, S is the flow speed of the gas and RTI (response time index) is a measure of the sensor's sensitivity to temperature change (a thermal inertia). The RTI of sprinkler heads is measured in a standard apparatus (see Heskestadand Smith [14]) for use in system design and activation prediction. Sprinkler head (activation) performance is classified by RTI value. For heat detectors space rating has a similar use and a correlation between space rating and RTI is made in NFPA 72E. This model (equation (1)) assumes that forced convection is the dominant mode of heat transfer. Heat loss due to radiation and conduction are assumed to be small.

Equation (1) is solved for each control volume using the implicit trapezoidal rule. As this equation is being solved, the time at which the sensor activates is also recorded. These contours, gas temperature activation times and link temperature activation times based on RTI values of 50, 100, 300 are used to determine the effect of sensor placement on activation time.

From examining these contours, several observations can be made which are discussed in the final section.

SUMMARY AND CONCLUSIONS

Many of the following observations are obvious at least in hindsight but are noted because of the impact they have on sensor siting strategies and related codes.

Beams trap flow. When beams are sufficiently deep no flow gets into adjacent channels. This can result in earlier sensor activation times under beamed ceilings than under smooth ceilings provided that a sensor is located in every channel.

A related observation is that beams cause flow near the ceiling to slow down and as a result, temperatures are warmer near the ceiling for beam cases than for non-beam cases. Figure 6 shows a cross-section near the ceiling for several cases with different beam depths. Note that the activation region for the 0.10 m (4 in) and 0.20 m (8 in) beam depth cases is larger than the activation region for the smooth ceiling.

Due to the dependence on $\sqrt{\text{flow velocity}}$, heat detectors can be adversely affected by the reduced ceiling jet velocity.

The activation time[6] of sensitive sensors (smoke detectors or RTI=50 heat detectors) is independent of fire growth rate. For smoke detectors in Figure 7 the response surface for when a sensor activates by the time the fire has reached 1.0 MW are essentially the same. A similar behavior is observed for low thermal inertia (RTI=50) heat sensors. This was not observed however for heat sensors with high thermal inertia (RTI>100).

Conditions in beam channels may be equivalent[7] to conditions under beams. Figure 6 shows smoke detector response volumes for various beam depths. Similar figures showing smoke and heat detector response volumes for various beam depths, on center beam spacings, ceiling heights and fire sizes are presented in Forney et al. [6]. The surface of the response volumes represent a region where the sensor behaves (*ie* activates in the same time) in the same way. The modeling results are symmetric with respect to the right hand edge of these plots. The contour plot in Figure 5 is essentially the same as the third contour in Figure 6 except that the symmetric portion is included.

It is presumed that the two beams and one channel to the right of the symmetry plane will also activate a sensor. The results of all of the parametric variations on sensor spacing are summarized in Table 2. An entry in this table is determined by examining the corresponding contour plot. If the contour plot shows that a sensor has activated below 2 beams and within 2 channels then the corresponding table entry will be b4/c3. The notation bi or cj means put a sensor under every i'th beam or in every j'th channel. For example, the dark grey contours are in the middle three channels and under the middle four beams in Figure 5. Therefore the entry under case B8, 100 kW should be b4/c3. The b*i*/c*j* can be obtained for each contour plot by reflecting the plot about the plane of symmetry (the right edge of the figure) in the same way that Figure 5 was generated.

The optimum sensor locations relative to regularly spaced obstructions (beams or joists) as a function of beam spacing, depth, fire size, and ceiling height are summarized in Table 2. The F1, F2 and F3 entries under the smoke detector column are supported by Figure 2. The B4, B8, B12 and B24 entries are supported by Figure 3. Other entries in this table were determined using contour plots similar to those presented in these two two figures. Figures for each table entry can be found in Forney et al. [6]. Each case summarized in Table 2 was run for 300 seconds. A medium growth rate fire reached a design size of 100 kW and 1 MW in 85 and 268 seconds respectively. The dark grey shadings in the preceding figures then refer to regions where a sensor activates before the fire reaches 100 kW or equivalently where it activates before 85 seconds. Similarly, the light grey shadings refer to where a sensor will activate before the fire reaches 1 MW or equivalently before 268 seconds. Thus, a device positioned at any location on the constant response volume

[6] time normalized to when a fire reaches 1 MW

[7] in the sense that a sensor will activate in the same time

Table 1: Description of Numerical Experiments Performed in Case Study

Cases	fire growth rate	beam depth	beam spacing	ceiling height
F1	slow	.305 m (1 ft)	1.22 m (4 ft)	3.35 m (11 ft)
F2	medium	.305 m (1 ft)	1.22 m (4 ft)	3.35 m (11 ft)
F3	fast	.305 m (1 ft)	1.22 m (4 ft)	3.35 m (11 ft)
W4	medium	.305 m (1 ft)	1.22 m (4 ft)	3.35 m (11 ft)
W5	medium	.305 m (1 ft)	1.52 m (5 ft)	3.35 m (11 ft)
W6	medium	.305 m (1 ft)	1.83 m (6 ft)	3.35 m (11 ft)
W7	medium	.305 m (1 ft)	2.13 m (7 ft)	3.35 m (11 ft)
W8	medium	.305 m (1 ft)	2.44 m (8 ft)	3.35 m (11 ft)
B0	medium	0.00 m (0 in)	1.22 m (4 ft)	3.35 m (11 ft)
B4	medium	0.10 m (4 in)	1.22 m (4 ft)	3.35 m (11 ft)
B8	medium	0.20 m (8 in)	1.22 m (4 ft)	3.35 m (11 ft)
B12	medium	0.305 m (1 ft)	1.22 m (4 ft)	3.35 m (11 ft)
B24	medium	0.610 m (2 ft)	1.22 m (4 ft)	3.35 m (11 ft)
H12	medium	.305 m (1 ft)	1.22 m (4 ft)	3.35 m (11 ft)
H15	medium	.305 m (1 ft)	1.22 m (4 ft)	4.57 m (15 ft)
H19	medium	.305 m (1 ft)	1.22 m (4 ft)	5.79 m (19 ft)
H22	medium	.305 m (1 ft)	1.22 m (4 ft)	6.71 m (22 ft)
H25	medium	.305 m (1 ft)	1.22 m (4 ft)	7.62 m (25 ft)
H28	medium	.305 m (1 ft)	1.22 m (4 ft)	8.53 m (28 ft)

Table 2: Summary of spacing recommendations (bj = under every j'th beam, ci= in every i'th channel) for thermal sensors based on an activation temperature of $57°C$ $(135°F)$ and for smoke detectors based on an activation temperature rise of $13°C$ $(23.4°F)$

Case	Thermal Detector						Smoke Detector	
	RTI = 50		RTI = 100		RTI = 300			
	100 kW	1.0 MW	100 kW	1.0 MW	100 kW	1.0 MW	100 kW	1.0 MW
F1	-	b4/c3	-	b4/c3	-	c1	b2/c3	b6/c5
F2	-	b2/c3	-	b2/c3	-	c1	b2/c3	b6/c5
F3	-	c3	-	c1	-	-	c1	b6/c5
W4	-	b2/c3	-	b2/c3	-	c1	b2/c3	b6/c5
W5	-	b2/c3	-	b2/c1	-	c1	b2/c1	b4/c5
W6	-	b2/c3	-	c1	-	c1	c1	b4/c5
W7	-	b2/c3	-	c1	-	c1	c1	b4/c5
W8	-	c1	-	c1	-	c1	c1	b4/c5
B4	-	b4/c5	-	b4/c5	-	c1	b4/c5	b6/c5
B8	-	b4/c5	-	b4/c3	-	c1	b4/c3	b6/c5
B12	-	b2/c3	-	b2/c3	-	c1	b2/c3	b6/c5
B24	-	c1	-	c1	-	c1	c1	b2/c3
H11	-	b2/c3	-	b2/c3	-	c1	b2/c3	b6/c5
H15	-	c1	-	c1	-	-	c1	b6/c5
H19	-	c1	-	c1	-	-	-	b6/c5
H22	-	c1	-	-	-	-	-	b6/c5
H25	-	-	-	-	-	-	-	b6/c5
H28	-	-	-	-	-	-	-	b4/c5

would activate at the same time.

By utilizing the entries in the table along with the related beam spacing, a spacing distance can be obtained. For example, in any of the B cases (beam spacing 1.22 m (4 ft)) a c3 entry would relate to a sensor spacing of 3.6 m (12 ft). In most cases for smoke detectors these results will require fewer sensors and simpler installations (with an attendant cost savings) at no reduction of performance or safety. For thermal activated sensors the effect of local flow velocities is such that more (closer spaced) sensors are needed to provide activation times equivalent to smooth ceiling cases.

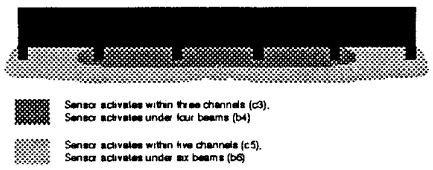

FIGURE 5: Example of shaded contour plot that includes both sides of the symmetry plane

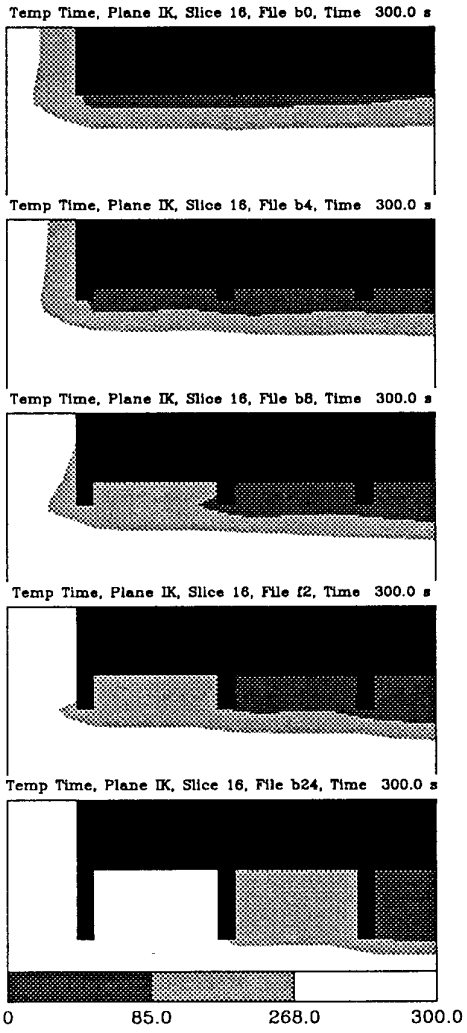

FIGURE 6: Shaded contour plot of smoke detector response volumes for various beam depths: 0.0 m (0 in), 0.10 m (4 in), 0.20 m (8 in), 0.30 m (12 in), 0.61 m (24 in)with 3.35 m (11 ft) ceiling height, 1.22 m (4 ft) beam spacingand medium fire. Dark and light grey denotes where a sensor activates before the fire reaches 100 kW and 1.0 MW respectively. White denotes where the sensor would not activate. Activation criteria: when the gas temperature rises $13°C$ above ambient.

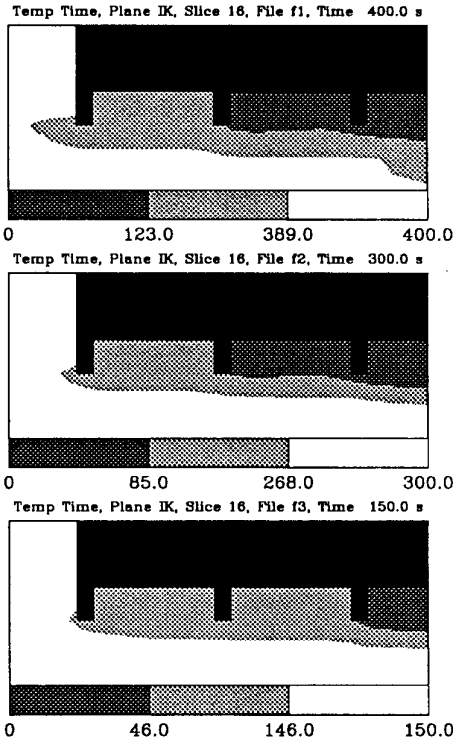

FIGURE 7: Shaded contour plot of smoke detector response volumes for various fire sizes: slow (denoted f1, reaches 1.0 MW in 389 seconds), medium (denoted f2, reaches 1.0 MW in 268 seconds), fast (denoted f3, reaches 1.0 MW in 146 seconds)with 0.305 m (12 in) beam depth, 3.35 m (11 ft) ceiling height and 1.22 m (4 ft) beam spacing. Dark and light grey denotes where a sensor activates before the fire reaches 100 kW and 1.0 MW respectively. White denotes where the sensor would not activate. Activation criteria: when the gas temperature rises $13°C$ above ambient.

REFERENCES

[1] G. Heskestad and M. A. Delichatsios. Environments of Fire Detectors - Phase I: Effect of Fire Size, Ceiling Height and Material, Volume I. Measurements. NBS-GCR-77-86, National Institute of Standards and Technology, 1977.

[2] G. Heskestad and M. A. Delichatsios. Environments of Fire Detectors - Phase I: Effect of Fire Size, Ceiling Height and Material, Volume II. Analysis. NBS-GCR-77-95, National Institute of Standards and Technology, 1977.

[3] G. Heskestad and M. A. Delichatsios. Environments of Fire Detectors - Phase II: Effect of Ceiling Configuration. Volume I. Measurements. NBS-GCR-78-128, National Institute of Standards and Technology, 1978.

[4] G. Heskestad and M. A. Delichatsios. Environments of Fire Detectors - Phase II: Effect of Ceiling Configuration. Volume I. Analysis. NBS-GCR-78-129, National Institute of Standards and Technology, 1978.

[5] Glenn P. Forney, William D. Davis, and John H. Klote. Simulating the effect of beamed ceilings on smoke flow, Part I. Comparison of numerical and experimental results. NISTIR 4994, National Institute of Standards and Technology, 1992.

[6] Glenn P. Forney, Richard W. Bukowski, and William D. Davis. Simulating the effect of flat beamed ceilings on detector and sprinkler response, 1993. Available from the National Fire Protection Association, Batterymarch Park, Quincy, MA.

[7] B.E. Launder and D.B. Spalding. The numerical computation of turbulent flows. *Computer Methods in Applied Mechanics and Engineering*, 3:269–289, 1974.

[8] NFPA 72E, Automatic Fire Detectors, 1987 edition, 1987.

[9] Glenn P. Forney and William D. Davis. Analyzing strategies for eliminating flame blow-down occuring in the Navy's 19F4 fire fighting trainer. NISTIR 4825, National Institute of Standards and Technology, 1992.

[10] Ronald F. Boisvert, Sally E. Howe, David K. Kahaner, and Jeanne L. Springmann. Guide to Available Mathematical Software. NISTIR 90-4237, National Institute of Standards and Technology, 1990. Also available as PB90-216508/AS, National Technical Information Service, Springfield, VA 22161.

[11] Carl de Boor. *A Practical Guide to Splines*. Springer-Verlag, New York, 1978.

[12] Carl de Boor. Efficient computer manipulation of tensor products. *ACM Transactions on Mathematical Software*, 5:173–182, 1978.

[13] Gunnar Heskestad. Fire plumes. In Phillip J. DiNenno, editor, *SFPE Handbook of Fire Protection Engineering*, chapter I-6. McGraw-Hill Book Company, New York, first edition, 1989.

[14] Gunnar Heskestad and Herbert F. Smith. Investigation of a new sprinkler sensitivity approval test: The plunge test. Technical Report Serial No. 22485 2937, Factory Mutual Research Corporation, Norwood, MA, 1976. RC 76-T-50.